



THE UNIVERSITY *of* EDINBURGH

Edinburgh Research Explorer

## The bond-behaviour of CFRP-to-concrete bonded joints under fatigue loading: A damage accumulation model

**Citation for published version:**

Zhou, H, Zhang, SS, Fernando, D & Huang, T 2023, 'The bond-behaviour of CFRP-to-concrete bonded joints under fatigue loading: A damage accumulation model', *Engineering Fracture Mechanics*, vol. 284, 109272, pp. 109272. <https://doi.org/10.1016/j.engfracmech.2023.109272>

**Digital Object Identifier (DOI):**

[10.1016/j.engfracmech.2023.109272](https://doi.org/10.1016/j.engfracmech.2023.109272)

**Link:**

[Link to publication record in Edinburgh Research Explorer](#)

**Document Version:**

Peer reviewed version

**Published In:**

Engineering Fracture Mechanics

**General rights**

Copyright for the publications made accessible via the Edinburgh Research Explorer is retained by the author(s) and / or other copyright owners and it is a condition of accessing these publications that users recognise and abide by the legal requirements associated with these rights.

**Take down policy**

The University of Edinburgh has made every reasonable effort to ensure that Edinburgh Research Explorer content complies with UK legislation. If you believe that the public display of this file breaches copyright please contact [openaccess@ed.ac.uk](mailto:openaccess@ed.ac.uk) providing details, and we will remove access to the work immediately and investigate your claim.



1 **The bond-behaviour of CFRP-to-concrete bonded joints under fatigue loading: a**  
2 **damage accumulation model**

3 Hao Zhou<sup>1</sup>, Shishun Zhang<sup>2</sup>, Dilum Fernando<sup>3,\*</sup>, Tianli Huang<sup>1</sup>

4 <sup>1</sup>School of Civil Engineering, Central South University, Changsha 410075, China

5 <sup>2</sup>School of Civil and Hydraulic Engineering, Huazhong University of Science and Technology,  
6 Wuhan 430074, China

7 <sup>3</sup>School of Engineering, University of Edinburgh, Edinburgh, EH9 3FB, Scotland, UK

8 Corresponding author: dilum.fernando@ed.ac.uk

9

10 **Abstract:**

11 This paper presents a theoretical study aimed at predicting the behaviour of carbon fibre reinforced  
12 polymer-to-concrete bonded joints under fatigue-cyclic loading. A model considering the plastic  
13 deformations of the interface, the damage, and the damage accumulation due to fatigue-cyclic loading  
14 is proposed. The damage accumulation model is calibrated through the experimental bond-slip  
15 relation. Then, a numerical algorithm is formulated to simulate the fatigue bond behaviour using the  
16 calibrated damage accumulation model. Numerical simulation was found to provide conservative  
17 predictions for fatigue life, which was attributed to the neglect of beneficial effects from the  
18 compression stress state near the loaded end in the single-shear pull-off test.

19 **Keywords:** CFRP strengthening; bond behaviour, fatigue loading, damage accumulation model

20

## 21 **1 Introduction**

22 Carbon fibre reinforced polymer (CFRP) strengthening of reinforced concrete (RC) structures to  
23 increase flexural and shear capacities has become a popular technique amongst the construction  
24 engineers due to its many advantages such as high strength-to-weight ratio, ease of application, and  
25 less disturbance to traffic [1, 2]. Amongst the numerous strengthening techniques using CFRPs, the  
26 externally bonded (EB) CFRP laminate strengthening technique that requires minimal efforts to  
27 implement has been the most popular technique. Performance of RC structures strengthened using  
28 EB CFRP relies on the interfacial shear stress transfer mechanism of the CFRP-to-concrete (FC)  
29 bonded joints [3]. Therefore, understanding the behaviour of FC bonded joints is of key significance.  
30 As a result, many efforts have been devoted to understanding and predicting the bond behaviour of  
31 FC bonded joints [4-8]. Design theories have been well established to predict the behaviour of FC  
32 bonded joints under quasi-static monotonic loading [4, 5]. In these prediction models, a bond-slip  
33 relation which describes the relation between the interfacial shear stress and the relative displacement  
34 between the CFRP and concrete substrate, is commonly used for modelling the behaviour of FC  
35 bonded joints under monotonic loading [5,9]. In such bond-slip models, a damaged elasticity  
36 assumption (i.e., load is assumed to always unload to zero at zero slip) is often made for defining  
37 damage evolution.

38 Many EB CFRP strengthened RC structures, such as bridge girders are likely to be subjected to  
39 repeated loading. Such repeated loading can be generally categorized into quasi-static cyclic loading  
40 and fatigue-cyclic loading according to the loading frequency. For simplicity, the former will be  
41 termed as cyclic loading and the latter as fatigue loading in this paper. Compared to the research on  
42 the bond behaviour under monotonic loading, only limited research has been carried out so far on  
43 understanding the behaviour of FC bonded joints under cyclic loading [9-14]. Existing experimental  
44 investigations have shown that when subjected to cyclic loading, FC bonded joints also fail within  
45 concrete (i.e. cohesion failure within concrete) similarly to those joints subjected to monotonic  
46 loading [14].

47 Experimentally derived bond-slip relations under cyclic loading showed clear damage plasticity (i.e.  
48 reduction in unloading stiffness due to damage and residual slip at zero load during unloading  
49 showing plastic deformations) behaviour [11, 14, 15] therefore shows the commonly used damage  
50 elasticity assumption in representing the cyclic bond behaviour is not accurate [3, 16]. Several  
51 analytical models have been proposed to predict the cyclic bond behaviour of the FC bonded joints  
52 considering damaged plasticity [12-14]. Different from bond-slip relations under monotonic loading,  
53 bond-slip relations under cyclic loading require damage parameters to be defined considering both  
54 damage and plasticity during unloading/reloading within the softening range. Zhou et al. [14] pointed  
55 out several shortcomings of the existing models and proposed the first thermodynamically consistent  
56 bond-slip relation for FC bonded joints under cyclic loading. However, existing experimental studies  
57 on FC bonded joints under fatigue loading have shown that failure modes are more complex than that  
58 of FC bonded joints under monotonic or cyclic loading [17-25], thus bond-slip models derived for  
59 monotonic or cyclic loading cannot be directly applied to FC bonded joints under fatigue loading.

60 Different failure modes including cohesion failure within the concrete, cohesion failure within the  
61 adhesive, adhesion failure at the CFRP-adhesive bi-material interface, adhesion failure at the  
62 concrete-adhesive bi-material interface, and interlaminar failure within the CFRP laminate were  
63 observed in FC bonded joint tests under fatigue loading [18, 20-23, 26]. Amongst the failure modes  
64 observed, adhesion failures are subjected to the quality of surface preparation. However, studies  
65 reporting the adhesion failures often did not report surface quality measurements or sufficient details  
66 of the adopted surface preparation methods. Therefore, it is difficult to assess if the adhesion failure  
67 was driven by the poor surface quality. On the otherhand, existing research has shown that with  
68 adequate surface preparation, adhesion failure modes of the FC bonded joints (i.e. adhesion failure at  
69 the CFRP-adhesive and the concrete-adhesive bi-material interfaces) can be avoided [26]. Once  
70 adhesion failures are avoided, failure mode under fatigue loading was found to be dependent on the  
71 concrete strength, the CFRP laminate type and the maximum fatigue load level [27]. To date the exact  
72 reasons for complex failure modes observed under fatigue loading remain largely unknown. More

73 studies are required to better understand the change of failure modes in FC bonded joints under fatigue  
74 loading. Nonetheless, while the effect of CFRP laminate type on the overall fatigue performance is  
75 not clear, the selection of a certain type of CFRP laminate (e.g. MasterBrace Laminate) was found to  
76 to avoid the CFRP interlaminar failure and the failures were limited to cohesion failure within  
77 concrete or cohesion failure within adhesive [27]. Experimental studies of FC bonded joints under  
78 fatigue loading showed a decrease in the slope of the load-displacement curve with the increasing  
79 number of loading cycles [19-26]. Softening of the interface and the gradual debonding of the CFRP  
80 laminate from the concrete substrate are believed to be the reasons for the observed degradation of  
81 stiffness of the load-displacement curves.

82 It is common to assess the performance of a bonded joint in terms of its fatigue life (i.e. number of  
83 loading cycles the bonded joint can sustain), thus has been the key focus of the majority of the  
84 published work on FC bonded joints under fatigue loading [18, 21, 25, 28, 29]. To the best of the  
85 author's knowledge, only two studies have been published so far on the experimental bond-slip  
86 behaviour of FC bonded joints under fatigue loading [23, 26]. Both studies showed an obvious  
87 damage accumulation in unloading/reloading stiffness of the bond-slip relation because of the fatigue  
88 loading. Existing experimental investigations on FC bonded joints under fatigue loading [27] have  
89 demonstrated that if elastic interfacial shear stresses are less than 80% of the maximum interfacial  
90 shear strength, fatigue loading would not cause any damage. When loaded beyond this stress level,  
91 damage due to fatigue will initiate and starts to accumulate. A similar conclusion can be found in Al-  
92 Saoudi et al. [30] in which the fatigue damage threshold value of the stress was found to be 75% of  
93 the maximum interfacial shear strength under monotonic loading.

94 Several theoretical models have been proposed to predict the fatigue life of FC bonded joints [22, 25,  
95 26, 31, 32], the rate of debonding [18, 28], and the bond-slip relation under fatigue loading [13, 23,  
96 33]. Among which, Zhu et al. [26] and Li et al. [22] expressed the fatigue life of FC bonded joints as  
97 a function of the loading amplitude and the concrete compressive strength. However, the fatigue life  
98 of the bonded joints is also affected by the interface geometry (e.g., CFRP laminate thickness,

99 adhesive thickness) which affects the interfacial stress significantly. Therefore, both models cannot  
100 be applied for bonded joints of different geometries. Carrara and De Lorenzis [13] proposed a  
101 damage-plasticity model to capture the behaviour of the bonded interface under fatigue loading. Their  
102 model assumed unloading of the slip with zero interfacial shear stress. However, this assumption was  
103 later proven to be unreasonable by experimental results of FC bonded joints under cyclic loading [14].  
104 Recent study by Zhang et al. [33] presented a mix-mode cohesive zone model to simulate the bond  
105 behaviour of FC bonded joints under fatigue loading. Stiffness degradation of the traction-separation  
106 curves was not related to the number of loading cycles. Empirical-based equations were developed  
107 for load degradation as a function of the number of loading cycles. Such a model however does not  
108 appropriately consider the fatigue damage of the interface as a function of the loading applied to the  
109 interface, thus cannot be used in general for modelling fatigue behaviour of any FC bonded interface.  
110 It should be noted that none of the existing models considered the possibility of fracture surface  
111 moving from one constituent to another. As the interfacial fracture work is directly related to the  
112 constituent where the fracture would occur, a change in the failure mode affects the total fracture  
113 work thus the damage process. Therefore, if the fracture path is different, models ignoring the failure  
114 mode change cannot be directly applied.

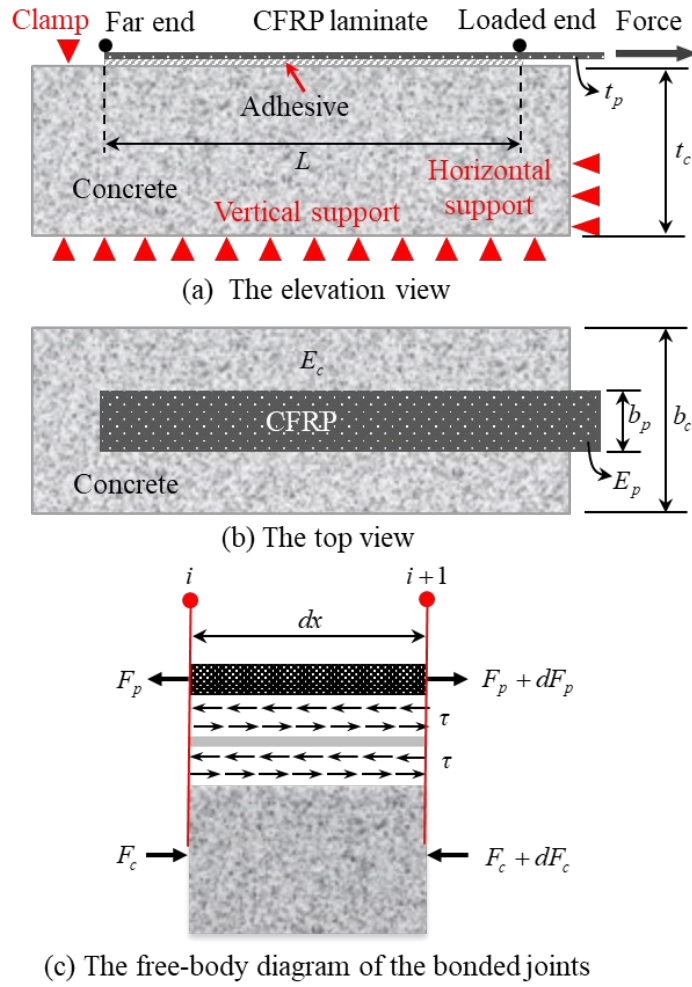
115 Against this background, this paper presents a theoretical study aimed at developing a bond-slip  
116 relation for FC bonded joints under fatigue loading, when the failure mode is cohesion failure within  
117 concrete. The present study is built upon the previous experimental work carried out by the authors  
118 on FC bonded joints subjected to fatigue loading [27]. Only the “cohesion failure within concrete”  
119 failure mode was considered due to lack of data available on FC bonded joints subjected to fatigue  
120 loading and failing in other failure modes. In the present study, a finite difference (FD) algorithm was  
121 firstly formulated to simulate the bond behaviour of FC bonded joints under fatigue loading. Then, a  
122 path-defined model was proposed to simulate the unloading and reloading of bond-slip relation under  
123 fatigue loading. Based on the experimental results of FC bonded joints failed within concrete, the  
124 damage accumulation rate was calibrated through regression analysis and was implemented in the

125 proposed FD algorithm. The load-displacement curve and the local bond-slip relation from the  
126 numerical predictions were compared with test results.

## 127 **2 The proposed model**

### 128 *2.1 Simulation of the CFRP-to-concrete bonded joints under fatigue loading*

129 The bond behaviour of FC bonded joints is often investigated through a single-shear pull-off test (Fig.  
130 1). By assuming that the interfacial shear stresses are uniform through the thickness of the adhesive  
131 layer and ignoring the bending and longitudinal normal stresses in the adhesive layer, the free body  
132 diagram of an indefinite segment can be drawn as Fig. 1c. These assumptions, also commonly adopted  
133 in other research, were shown to have a negligible effect on the simulation of the behaviour of FC  
134 bonded joints under mode II loading [7, 12, 34]. To simulate the bond behaviour of FC bonded joints  
135 under fatigue loading, the FD method proposed by Carrara and Ferretti [34] was modified to account  
136 for the change in bond-slip relation when fatigue loading is applied. Detailed FD method is presented  
137 below.



138

139

**Fig.1.** Idealized CFRP-to-concrete (FC) bonded joints

140

According to the force equilibrium of the CFRP element shown in Fig. 1c, the following differential

141

equation can be established:

142

$$\frac{dF_p}{dx} = \tau b_p \quad (1)$$

143

where  $F_p$  and  $b_p$  are the axial force and width of the CFRP plate respectively,  $\tau$  is the interfacial

144

shear stress acting at the bi-material interface with segment length  $dx$ .

145

The relative displacement between the CFRP plate and the concrete substrate, i.e., slip ( $\delta$ ) can be

146

written as follows:

147

$$\delta = u_p - u_c \quad (2)$$



148 Where  $u_p$  and  $u_c$  are the displacements of CFRP plate and concrete at a given position of the  
149 bonded joints respectively.

150 For the CFRP laminate and the concrete under axial loading, the constitutive relation can be written  
151 as:

$$152 \quad \sigma_p = E_p \frac{du_p}{dx} \quad (3)$$

$$153 \quad \sigma_c = E_c \frac{du_c}{dx} \quad (4)$$

154 where  $E_p$  and  $E_c$  are the elastic moduli of the CFRP plate and concrete respectively, and  $\sigma_p$  and  $\sigma_c$   
155 are the axial stresses of the CFRP plate and the concrete respectively. The axial stresses of the CFRP  
156 plate and the concrete can be also written as:

$$157 \quad \sigma_p = \frac{F_p}{A_p} \quad (5)$$

$$158 \quad \sigma_c = \frac{F_c}{A_c} \quad (6)$$

159 where  $F_c$  is the axial force applied on the concrete block,  $A_p$  and  $A_c$  are the sectional areas of CFRP  
160 laminate and concrete substrate respectively. According to the force equilibrium at any section, the  
161 following equation can be derived:

$$162 \quad F_p + F_c = 0 \quad (7)$$

163 From Eqs (2)-(7), the following equation can be derived:

$$164 \quad \frac{d\delta}{dx} = \left( \frac{1}{E_p A_p} + \frac{1}{E_c A_c} \right) F_p \quad (8)$$

165 Dividing the whole bonding interface into  $n$  number of segments, Eqs (1) and (8) at each segment  $i$   
 166 (Fig.1c) can be approximated as:

$$167 \quad \frac{F_p^{i+1} - F_p^i}{h_i} = \frac{1}{2} [\tau^{i+1} + \tau^i] b_p \quad (9)$$

$$168 \quad \frac{\delta^{i+1} - \delta^i}{h_i} = \frac{1}{2} \left( \frac{1}{E_p A_p} + \frac{1}{E_c A_c} \right) (F_p^{i+1} + F_p^i) \quad (10)$$

169 where  $h_i$  is the length of the segment,  $\delta^i, \tau^i, F_p^i$  are the slip, interfacial shear stress and axial force of  
 170 CFRP at node  $i$ , respectively. When a bilinear bond-slip relation is adopted, the interfacial shear stress  
 171 can be calculated as:

$$172 \quad \tau^i = \tau_f^i + K_t^i (\delta^i - \delta_1^i) \quad (11)$$

173 where  $\tau_f^i$  and  $K_t^i$  are the peak shear stress and the tangential stiffness of the bond-slip relation in a  
 174 given loading cycle.  $\delta_1^i$  is the slip value at the peak shear stress at node  $i$  in a particular loading cycle.

175 Experimental observations showed that when fatigue loading was stopped and followed by monotonic  
 176 loading, the bond behaviour has followed the envelope bond-slip relation under monotonic loading  
 177 [27]. Therefore, it is assumed that for slip values greater than  $\delta_1^i$ , the slope of the softening curve will  
 178 be the same as the softening branch of the bond-slip curve under monotonic loading, i.e.  $K_s$ .

179 Therefore,  $K_t^i$  can be calculated as:

$$180 \quad K_t^i = \begin{cases} (1-D^i) K_e & \text{if } \delta_e^i < \delta < \delta_1^i \\ K_s & \text{if } \delta_1^i < \delta < \delta_f^i \\ 0 & \text{if } \delta_f^i < \delta \end{cases} \quad (12)$$

181 where  $K_e$  and  $K_s$  are the initial tangential stiffness in the ascending branch and the slope of the  
 182 softening branch of the bond-slip relation respectively (Fig. 2),  $D^i$  is the damage parameter at node

183  $i$ , and  $\delta_1^i, \delta_e^i$ , and  $\delta_f^i$  are the slip values at the peak shear stress, zero shear stress and the full damage  
184 point at node  $i$  respectively. Experimental studies showed that once damage initiates, the value of the  
185  $D^i$  increases gradually until the full damage is reached [26]. Therefore, a model to define the  
186 variation of  $D^i$  (i.e., a damage accumulation model presented in Section 2.2) in Eq. (12) is necessary.  
187 During unloading, it is possible that interfacial shear stress becomes negative. In such a case, the  
188 tangential stiffness can be found by using the centre-symmetrical point of the slip values with respect  
189 to  $\delta_e^i$ .

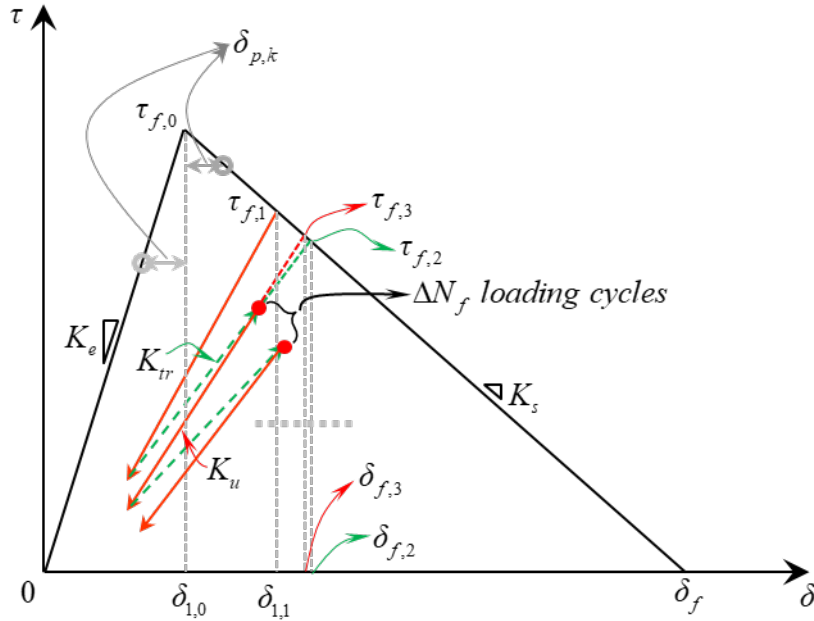
190 At the  $k^{th}$  step, substituting Eq. (11) into Eq. (9) gives:

$$191 \quad \frac{F_{p,k}^{i+1} - F_{p,k}^i}{h_i} = \frac{1}{2} \left[ \tau_{f,k}^{i+1} + K_{t,k}^{i+1} (\delta_k^{i+1} - \delta_{1,k}^{i+1}) + \tau_{f,k}^i + K_{t,k}^i (\delta_k^i - \delta_{1,k}^i) \right] b_p \quad (13)$$

192 As shown in Fig. 2, if the damage parameter is known, the maximum interfacial shear stress ( $\tau_{f,k}$ )  
193 and the corresponding slip value ( $\delta_{1,k}$ ) at different nodes in a particular loading cycle can be  
194 calculated and will be a constant value within that loading cycle. Therefore, Eq. (10) can be rewritten  
195 as:

$$196 \quad \frac{(\delta_k^{i+1} - \delta_{1,k}^{i+1}) - (\delta_k^i - \delta_{1,k}^i)}{h_i} = \frac{1}{2} \left( \frac{1}{E_p A_p} + \frac{1}{E_c A_c} \right) (F_{p,k}^{i+1} + F_{p,k}^i) - \frac{(\delta_{1,k}^{i+1} - \delta_{1,k}^i)}{h_i} \quad (14)$$

197



198

199

**Fig.2.** The proposed bond-slip model under fatigue loading.

200 Taking  $\delta_{d,k}^i = \delta_k^i - \delta_{1,k}^i$  and  $\delta_{d,k}^{i+1} = \delta_k^{i+1} - \delta_{1,k}^{i+1}$ , Eqs (13) and (14) can be expressed respectively as:

201

$$-\frac{F_{p,k}^i}{h_i} - \frac{1}{2} K_{t,k}^i \delta_{d,k}^i b_p + \frac{F_{p,k}^{i+1}}{h_i} - \frac{1}{2} K_{t,k}^{i+1} \delta_{d,k}^{i+1} b_p = \frac{1}{2} (\tau_{f,k}^{i+1} + \tau_{f,k}^i) b_p \quad (15)$$

202

$$-\frac{W}{2} F_k^i - \frac{\delta_{d,k}^i}{h_i} - \frac{W}{2} F_k^{i+1} + \frac{\delta_{d,k}^{i+1}}{h_i} = -\frac{(\delta_{1,k}^{i+1} - \delta_{1,k}^i)}{h_i} \quad (16)$$

203 where  $W = \frac{1}{E_p A_p} + \frac{1}{E_c A_c}$ . Expressing Eqs (15) and (16) in matrix form gives:

204

$$\begin{bmatrix} -\frac{1}{h_i} & -\frac{1}{2} K_{t,k}^i b_p & \frac{1}{h_i} & -\frac{1}{2} K_{t,k}^{i+1} b_p \\ -\frac{1}{2} W & -\frac{1}{h_i} & -\frac{1}{2} W & \frac{1}{h_i} \end{bmatrix} \begin{bmatrix} F_{p,k}^i \\ \delta_{d,k}^i \\ F_{p,k}^{i+1} \\ \delta_{d,k}^{i+1} \end{bmatrix} = \begin{bmatrix} \frac{1}{2} (\tau_{f,k}^{i+1} + \tau_{f,k}^i) b_p \\ -\frac{(\delta_{1,k}^{i+1} - \delta_{1,k}^i)}{h_i} \end{bmatrix} \quad (17)$$

205 Eq. (17) can be extended to model the full bond joint using the system of equations as:

206

$$\begin{bmatrix} \mathbf{J}_1 & \mathbf{Q}_1 & & & & \\ & \mathbf{J}_2 & \mathbf{Q}_2 & & & \\ & & \ddots & \ddots & & \\ & & & \mathbf{J}_i & \mathbf{Q}_i & \\ & & & & \ddots & \ddots \\ & & & & & \mathbf{J}_n & \mathbf{Q}_n \\ \mathbf{B}_1 & & & & & & \mathbf{B}_{n+1} \end{bmatrix} \begin{bmatrix} \mathbf{U}_1 \\ \mathbf{U}_2 \\ \vdots \\ \mathbf{U}_i \\ \vdots \\ \mathbf{U}_n \\ \mathbf{U}_{n+1} \end{bmatrix} = \begin{bmatrix} \mathbf{R}_1 \\ \mathbf{R}_2 \\ \vdots \\ \mathbf{R}_i \\ \vdots \\ \mathbf{R}_n \\ \mathbf{Z} \end{bmatrix} \quad (18)$$

207 The above equation can be also written as  $\mathbf{C} \times \mathbf{U} = \mathbf{R}$ , where  $\mathbf{C}$  is the coefficients matrix composed  
208 of  $\mathbf{J}_i$  and  $\mathbf{Q}_i$  which are given by:

209

$$\mathbf{J}_i = \begin{bmatrix} -\frac{1}{h_i} & -\frac{1}{2}K_{t,k}^i b_p \\ -\frac{1}{2}W & -\frac{1}{h_i} \end{bmatrix}, \quad \mathbf{Q}_i = \begin{bmatrix} \frac{1}{h_i} & -\frac{1}{2}K_{t,k}^{i+1} b_p \\ -\frac{1}{2}W & \frac{1}{h_i} \end{bmatrix} \quad (19)$$

210  $\mathbf{U}_i$  and  $\mathbf{R}_i$  in the matrixes  $\mathbf{U}$  and  $\mathbf{R}$  are given by:

211

$$\mathbf{U}_i = \begin{bmatrix} F_{p,k}^i \\ \delta_{d,k}^i \end{bmatrix}, \quad \mathbf{R}_i = \begin{bmatrix} \frac{1}{2}(\tau_{f,k}^{i+1} + \tau_{f,k}^i) b_p \\ -\frac{(\delta_{1,k}^{i+1} - \delta_{1,k}^i)}{h_i} \end{bmatrix} \quad (20)$$

212  $\mathbf{B}_1$  and  $\mathbf{B}_{n+1}$  in Eq. (18) are used to implement the boundary conditions, which are dependent on the  
213 load type (i.e., force or displacement) and  $\mathbf{Z}$  in Eq. (18) is the corresponding force or displacement  
214 vector at the loaded end. For fatigue loading of single shear pull-off tests on FC bonded joints  
215 presented in Zhou et al. [27], the force control method was used for the initial monotonic loading and  
216 the subsequent fatigue loading. However, the displacement control method was used for the final  
217 monotonic loading to failure. Therefore, both force and displacement boundary conditions should be  
218 considered in simulating the single-shear pull-off tests under fatigue loading presented in Zhou et al.  
219 [27]. For the test using force control, the boundary conditions are:

220 
$$\mathbf{B}_1 = \begin{bmatrix} 1 & 0 \\ 0 & 0 \end{bmatrix}, \quad \mathbf{B}_{n+1} = \begin{bmatrix} 0 & 0 \\ 1 & 0 \end{bmatrix}, \quad \mathbf{Z} = \begin{bmatrix} 0 \\ F^{n+1} \end{bmatrix} \quad (21)$$

221 Substituting the boundary conditions in Eq. (21) in to Eq. (18) and expanding the expression yields:

222 
$$1 \times F_{p,k}^1 + 0 \times \delta_{d,k}^1 + 0 \times F_{p,k}^{n+1} + 0 \times \delta_{d,k}^{n+1} = 0 \quad (22)$$

223 
$$0 \times F_{p,k}^1 + 0 \times \delta_{d,k}^1 + 1 \times F_{p,k}^{n+1} + 0 \times \delta_{d,k}^{n+1} = F_{p,k}^{n+1} \quad (23)$$

224 in which Eq. (22) represents no force is applied at the far end of the CFRP plate, while Eq. (23) means  
225 non-zero force is applied at the loaded end.

226 When the displacement-controlled loading is used, the boundary conditions can be considered as  
227 follows:

228 
$$\mathbf{B}_1 = \begin{bmatrix} 1 & 0 \\ 0 & 0 \end{bmatrix}, \quad \mathbf{B}_{n+1} = \begin{bmatrix} 0 & 0 \\ 0 & 1 \end{bmatrix}, \quad \mathbf{Z} = \begin{bmatrix} 0 \\ \delta_{d,k}^{n+1} \end{bmatrix} \quad (24)$$

229 Substituting the boundary conditions in Eq. (24) into Eq. (18) and expanding the expression yields:

230 
$$1 \times F_{p,k}^1 + 0 \times \delta_{d,k}^1 + 0 \times F_{p,k}^{n+1} + 0 \times \delta_{d,k}^{n+1} = 0 \quad (25)$$

231 
$$0 \times F_{p,k}^1 + 0 \times \delta_{d,k}^1 + 0 \times F_{p,k}^{n+1} + 1 \times \delta_{d,k}^{n+1} = \delta_{d,k}^{n+1} \quad (26)$$

232 which represent a displacement loading boundary condition applied at the loaded end of the CFRP  
233 plate.

234 Once  $\delta_{d,k}^i$  is solved iteratively, the interfacial shear slip at each node along the bonding length can  
235 be calculated from the following expression:

236 
$$\delta_k^i = \delta_{d,k}^i + \delta_{l,k}^i \quad (27)$$

237 and the interfacial shear stress can be determined from Eq. (11).

238 It can be seen from the above FD algorithm that the  $K_t^i$ , therefore  $D^i$  is critical in simulating the  
239 bond behaviour under fatigue cyclic loading. To account for the variation of  $K_t^i$  under fatigue loading,  
240  $D^i$  should be updated when fatigue cyclic loading is applied. A fatigue damage accumulation model,  
241 which describes the variation of  $D^i$  with fatigue loading is presented next.

## 242 ***2.2 The fatigue damage accumulation rate model***

243 Zhou et al. [14] presented a model to determine the damage parameter evolution of FC bonded joints  
244 during cyclic loading. In this model, the unloading and reloading were assumed to be the same, such  
245 an assumption is also adopted in Roe and Siegmund [35] and Zhang et al. [33]. However, actual  
246 loading and unloading behaviour of FC bonded joints demonstrate hysteretic loops [14]. Nonetheless,  
247 existing studies on FC bonded joints subjected to cyclic loading have demonstrated that ignoring the  
248 hysteretic behaviour in bond-slip models have negligible effects on the overall behaviour of the FC  
249 bonded joint [14, 32, 34]. However, assuming the same stiffness in loading and unloading cannot  
250 capture the damage accumulation unless the unloading reached the inverse softening region or the  
251 loading reached the envelope curve [14].

252 In the present study, in addition to the unloading/reloading curve, a transition path (dashed line in Fig.  
253 2) is defined to capture the damage accumulation between two unloading/reloading curves. Different  
254 from the reloading path, the transition path represents the damage parameter evolution for every  
255  $\Delta N_f$  number of fatigue loading cycles. In this study, the minimum  $\Delta N_f$  was taken as 20, as the  
256 experimental data in Zhou et al. [27] was recorded at every 20 cycles.

257 While finding the proper function to represent the damage parameter increment, the following  
258 characteristics of the bond-slip relation of FC bonded joints subjected to fatigue loading were  
259 considered:

260 (1) The damage under fatigue loading was assumed to occur only if the maximum interfacial  
261 shear stress is higher than 80% of the peak shear strength under monotonic loading [27]. When

262 a bi-linear bond-slip relation is employed in the simulation, the same ratio can be used for the  
 263 slip value at interfacial shear stress when the fatigue damage starts to accumulate.

264 (2) the damage accumulation rate was assumed to decrease with the damage level. Once the  
 265 fatigue loading was stopped and monotonic loading was applied, the bond-slip relationship  
 266 tends to follow the envelope bond-slip curve under monotonic loading.

267 With the above two considerations, the damage evolution law for both unloading/reloading and  
 268 transition stiffness is expressed as:

$$269 \quad \dot{D}_{ur/tr} = \alpha_{ur/tr} \times (1 - D_{ur/tr}) \times \exp(\beta_{ur/tr} \times D_{ur/tr}) \times \Delta \quad (28)$$

270 where  $\dot{D}_{ur/tr}$  is the damage accumulation rate for the unloading/reloading stiffness ( $D_{ur}$ ) or transition  
 271 stiffness ( $D_{tr}$ ) with respect to the loading cycles. It should be noted that the transition stiffness is the  
 272 slope of the curve representing the path between different loading cycles, thus it only carries a  
 273 numerical meaning in this study.  $\Delta$  is a parameter to account for loading amplitude effect on the  
 274 damage accumulation rate, and is given as:

$$275 \quad \Delta = \left[ \left\langle \frac{\delta_{\max}}{\delta_{1,0}} \right\rangle_+ \times \frac{\delta_{\max} - \delta_{\min}}{\delta_{1,0}} \right] \quad (29)$$

276 where  $\delta_{\max}$  and  $\delta_{\min}$  are the maximum and minimum slips the node can reach within the loading  
 277 cycle,  $\delta_{1,0}$  is the slip value corresponding to the maximum shear stress of the initial bond-slip relation  
 278 under monotonic loading, and  $\langle \rangle_+$  is an operator defined as:

$$279 \quad \langle \eta \rangle_+ = \begin{cases} \eta & \text{if } \eta \geq r_{cri} \\ 0 & \text{if } \eta < r_{cri} \end{cases} \quad (30)$$



280 where  $r_{cri}$  is the critical ratio when the fatigue damage starts to accumulate (in this study,  $r_{cri} = 0.8$  is  
 281 considered based on the test results presented in Zhou et al. [27]).  $r_{cri}$ ,  $\alpha_{ur/tr}$  and  $\beta_{ur/tr}$  are empirical  
 282 parameters calibrated from the experimentally obtained bond-slip relations under fatigue cyclic  
 283 loading.

284 As the damage accumulation rate under fatigue loading depends on both the current damage  
 285 parameter and the loading amplitude, the damage parameter in the unloading/reloading or transition  
 286 path under fatigue loading should be updated as follows:

$$287 \quad D_{ur/tr,tot}^i \Big|_t = D_{ur/tr}^i \Big|_{t-\Delta t} + \Delta t \times D_{ur/tr}^{\square} \Big|_{t-\Delta t} \quad (31)$$

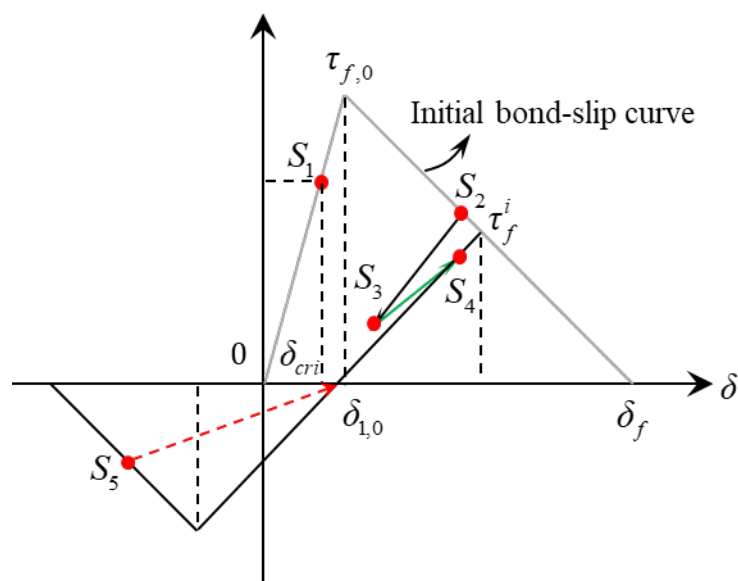
288 where  $t$  is the pseudo time, which could be the number of loading cycles, and  $\Delta t$  is the number of  
 289 loading cycles when the damage parameter is updated.  $D_{ur/tr}^i \Big|_{t-\Delta t}$  is the damage parameter of  
 290 unloading/reloading or transition stiffness at the  $i^{th}$  node at time  $t - \Delta t$ .

### 291 **2.3 The bond-slip relation of CFRP-to-concrete bonded joints subjected to fatigue loading**

292 A complete bond-slip relation of a FC bonded joint under fatigue loading is illustrated in Fig.3. As  
 293 mentioned previously, the damage parameter during the initial monotonic/cyclic loading of the  
 294 bonded joint can be calculated with the damage-plasticity model proposed in Zhou et al. [14]. In  
 295 which the damage parameter as a function of the ratio between the dissipated energy and the total  
 296 fracture energy. Once fatigue loading is applied, no damage will accumulate until the slip at that point  
 297 reach the critical value  $\delta_{cri} = r_{cri} \delta_{f,0}$  (S<sub>1</sub> in Fig.3) in which  $r_{cri} = 0.8$  is assumed according to previous  
 298 research by the authors group [27]. Beyond this slip, fatigue damage will start to accumulate. For a  
 299 point already in the softening stage (S<sub>2</sub> in Fig. 3), the damage parameter can be calculated from the  
 300 unloading/reloading stiffness, as the greater value between the value calculated from Eq. (31) and the  
 301 one from the damage-plasticity model under cyclic loading (i.e. Zhou et al. [14] model). It is assumed

302 that the change in damage parameter can only occur at the minimum slip point ( $S_3$  in Fig. 3) for the  
 303 transition stiffness, and the maximum slip point ( $S_4$  in Fig. 3) for the unloading/reloading stiffness

304 So far to the best of the authors' knowledge, no experimental data exists on FC bonded joints under  
 305 reversed cyclic loading, thus the behaviour of the FC bonded joints under reverse cyclic loading  
 306 remains largely unknown. In bond-slip relation of FC bonded joints, the total layers between the  
 307 underside of the CFRP laminate and the final fracture surface in concrete are considered as a single  
 308 layer. To date the most detailed explanation of fracture propagation process in FC bonded joints was  
 309 provided by Lu et al. [36]. Lu et al. [36] explained that under interfacial stresses, multiple diagonal  
 310 cracks may occur within concrete near the adhesive-concrete interface resulting in mesoscale columns.  
 311 At some stage, due to tensile stresses created by bending of those meso-scale columns, fracture  
 312 parallel to the axis of the bonded joint will occur. Reversal of the shear forces may create new fracture  
 313 lines orthogonal to the original diagonal cracks. In addition, reversal of the shear cracks will also  
 314 reverse the direction of bending of the meso-scale columns. Therefore, it is not possible to provide a  
 315 simple solution for reversal of bond-slip relation assuming reversal of plasticity. More investigations  
 316 are necessary to understand the mechanisms occurring at the bonded joints under reverse cyclic  
 317 loading.



318  
 319 **Fig.3.** Possible states of the nodes under fatigue loading.

320 For completeness of the model proposed in this paper, a damaged elasticity type of model was  
321 assumed when shear stress is reversed. This is highlighted in Fig. 3 by the reversal of the load to point  
322 S<sub>5</sub>. The residual fracture energy during the reverse loading was assumed to remain unchanged. This  
323 assumption of the reverse loading model should be updated once better data become available.

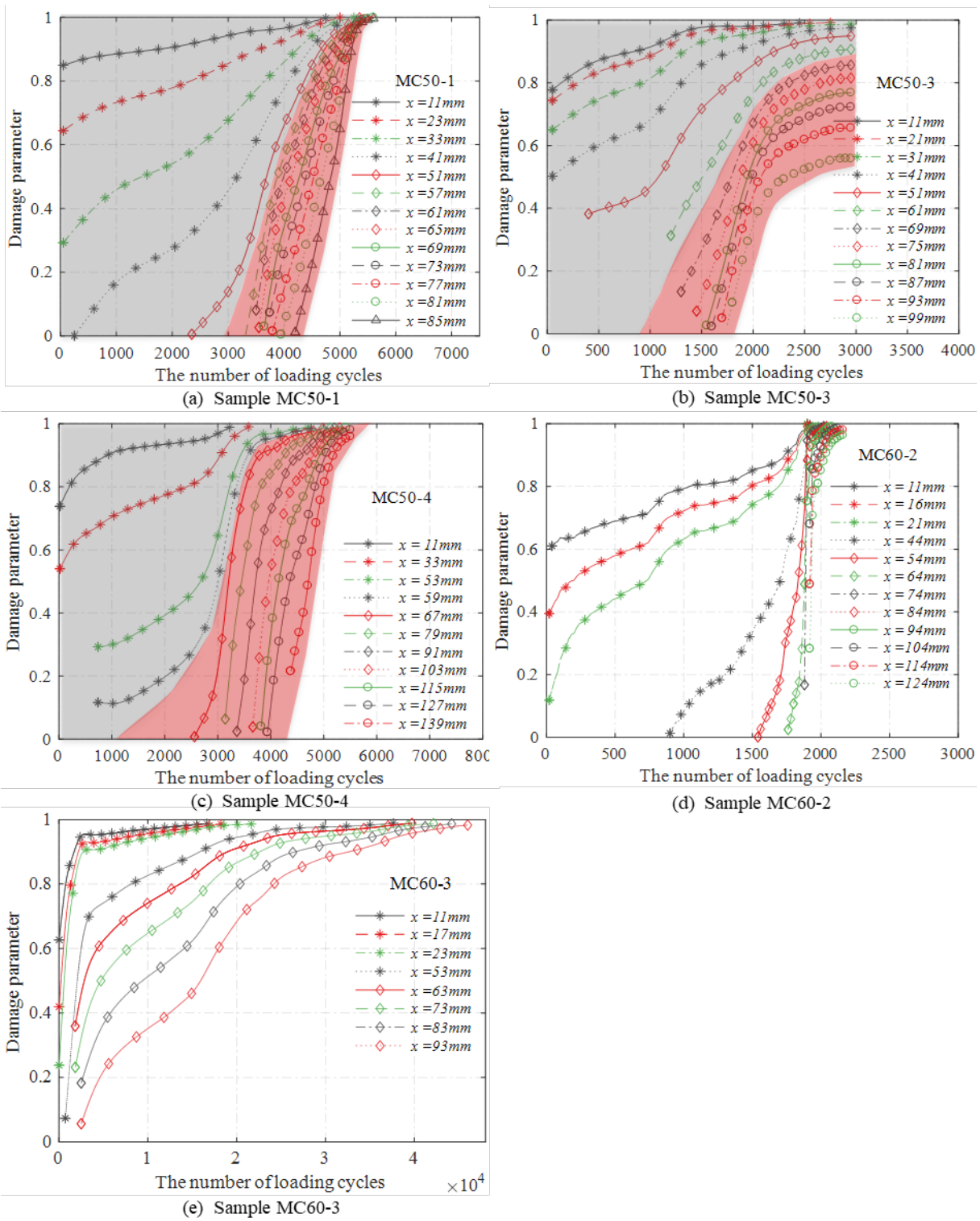
### 324 **3 Damage parameter calculation**

325 The fracture work of the FC bonded joints is related to the fracture surface/path. Therefore, when  
326 obtaining the bond-slip relationship of the bonded joints, it is important to ensure attention is given  
327 to the particular failure mode. Bond-slip behaviour of an interface failing through fracture of a certain  
328 surface cannot be used to simulate the behaviour of a bonded joints failing through another fracture  
329 surface. As mentioned, the damage-plasticity model used to calculate the initial damage parameter is  
330 for the bonded joints failed within concrete. Therefore, in the present study, only the fatigue bond  
331 behaviour of FC bonded joints failed within concrete is considered. The other failure modes such as  
332 the inter-laminar failure of CFRP plate is dependent on the matrix used in the manufacturing. Data  
333 available so far on FC bonded joints under fatigue loading failing in failure modes other than cohesive  
334 failure within concrete are inadequate to derive any meaningful conclusions. Therefore, the fatigue  
335 bond behaviour of such FC bonded joints failing in failures other than cohesive failure within concrete  
336 is considered outside the scope of this study. To calibrate the empirical parameters presented in Eq.  
337 (28), only the bond-slip relation of FC bonded joints failed in concrete under fatigue loading should  
338 be used.

339 In the present work, only the bond-slip relation from the tests in Zhou et al. [26] where samples failed  
340 in cohesion failure within concrete (i.e., MC50-1, MC50-3, MC50-4, MC60-2 and MC60-3) were  
341 used. Specifically, for sample MC50-3, only the data recorded before the failure mode shifted from  
342 cohesion failure within concrete to adhesion failure (i.e., before 3000 loading cycles) was used. With  
343 the above bond-slip relation under fatigue loading, the unloading/reloading and the transition damage

344 parameter in recorded cycles were calculated by following the same steps as presented in Zhou et al.  
345 [14].

346 The evolution of the transition stiffness damage parameter at different positions of the bonded joint  
347 is presented in Fig.4. The corresponding figures for the unloading/reloading stiffness damage  
348 parameter can be found in Zhou et al. [27] and Zhou [37]. Except for the sample MC60-3, the damage  
349 accumulation rate in all other samples increased with distance from the loaded end and stabilized  
350 after a certain distance (about 60mm away from the loaded end). A slower damage accumulation rate  
351 was observed in regions closer to the loaded end due to the existence of compressive stress (the grey  
352 hatched zone in Figs. 4(a)-(c)), while damage accumulation rate in regions far away from the loaded  
353 end was much larger (in the light red hatched zone in Figs. 4(a)-(c)). As debonding propagates,  
354 compressive stress will gradually reduce resulting in gradual increase of damage rate. As debonding  
355 propagates away from the loaded end, mode II stresses become dominant resulting in a more stable  
356 damage rate. Existing studies show that mode I and mode II stress ratio varies along the bonded joints  
357 [34, 38]. While complex stresses including compression and shear stress exists in regions close to the  
358 loaded end [34], interfacial stress state becomes mode II dominant as debonding propagates away  
359 from the loaded end [39]. The existence of compressive stress could lower down the damage  
360 propagation rate compared to that under pure mode II loading. Similar observations were also made  
361 in existing experimental studies [10, 40].



362

363 **Fig.4.** The transition stiffness damage parameter evolution at different locations with the number of  
 364 loading cycles.

365 For CFRP-to-concrete bonded joints made of 64MPa concrete, it was found that the damage  
 366 accumulation rate was significantly affected by the maximum fatigue load. A gradually increasing  
 367 damage rate was observed in the MC60-2 specimen as well as in the MC50-1, -3, and -4 specimens.

368 However, when debonding propagated approx. 54mm into the bond line away from the loaded end,  
369 sudden crack propagations resulted in a steep gradient of the damage parameter accumulation curves  
370 as shown in Figs. 4(a)-(d). For the specimen MC60-3 (Fig. 4(e)), the minimum load applied varied  
371 during the testing as 11%, 12.5%, 13.9% and 11% of the load-carrying capacity under monotonic  
372 loading, which can explain the variation in damage increase rates at different locations [27].

373 As only the modelling of the interfacial behaviour of FC bonded joints under mode II loading is aimed  
374 at in this paper, only the damage propagation curves from the region where damage propagation is  
375 dominated by mode II loading (i.e. the middle region of the bond length) were considered in  
376 calibrating the empirical parameters in Eq. (28). Considering the sudden cracking observed during  
377 the testing of the sample MC60-2 [26], data from that sample was excluded from the calibration. It is  
378 obvious from Fig. 4, that data from the middle region of the specimens provide a higher damage  
379 accumulation rate than the data from the end regions. Therefore, when using the data from the middle  
380 region of the bonded joints, the calibrated parameters will lead to a higher damage accumulation rate  
381 prediction than the actual in regions close to the loaded end. As the proposed model will be applied  
382 to the whole bonding interface, the fatigue life prediction can be expected shorter than the actual.

#### 383 **4 Calibration of the damage accumulation rate model under fatigue loading**

384 The damage parameter evolution curves from different locations of the bonded joints were used to  
385 determine the damage accumulation rate for both the unloading/reloading and transition stiffness as  
386 a function of the loading parameter ( $\Delta$ ) and the damage parameter ( $D_{ur}$  or  $D_{tr}$ ). The slip value ( $\delta_1$ )  
387 corresponding to the peak shear stress under monotonic loading was also obtained through the tests.  
388 With the above parameters, a nonlinear regression analysis was carried out using all the test data (Fig.  
389 5). As can be seen in Fig. 5, a higher damage accumulation rate results in lower values of the damage  
390 parameter, and the damage accumulation rate tends to decrease as the damage level increases. In  
391 addition, for a given damage state, a greater loading parameter will result in a higher damage  
392 accumulation rate. In other words, an increase in fatigue damage accumulation rate can be expected

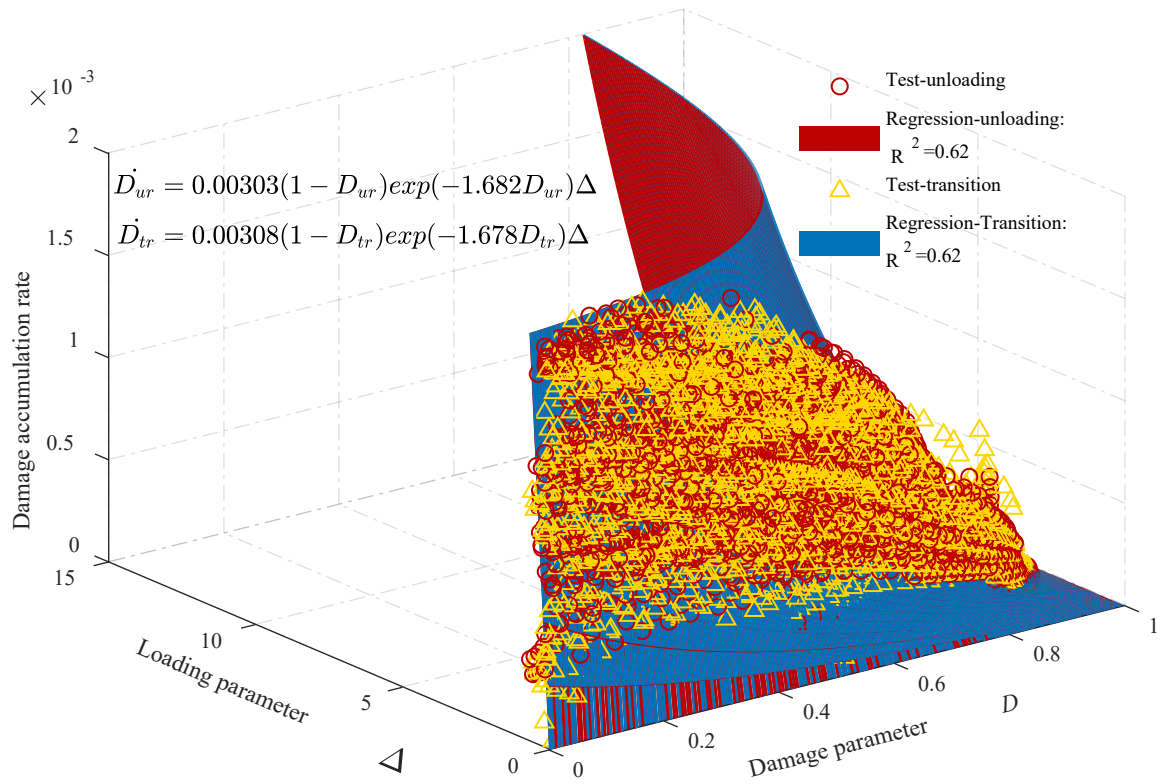
393 when a greater maximum load and a greater load amplitude are applied. Through a nonlinear  
394 regression analysis, expressions for the damage accumulation rate of unloading/reloading and  
395 transition stiffness are obtained as:

$$396 \quad \dot{D}_{ur} = 0.00303 \times (1 - D_{ur}) e^{(-1.678 D_{ur})} \Delta \quad (32)$$

$$397 \quad \dot{D}_{tr} = 0.00308 \times (1 - D_{tr}) e^{(-1.682 D_{tr})} \Delta \quad (33)$$

398 The degradation rate of the transition stiffness for a given damage parameter or loading parameter is  
399 slightly higher than that of the unloading/reloading stiffness. Significant scatter in data resulted in the  
400 relative low fitting score (0.66 and 0.64 represented by the adjusted R-square value). Such variance  
401 can be attributed to the dynamic cracking in the FC bonded joints. Typically, during damage  
402 propagation, a crack of a certain bonding length can occur at any given time. Inhomogeneity in the  
403 concrete microstructure as well as the number of micro cracks at any given stage influence the crack  
404 propagation, therefore may lead to different crack propagation rates. However, in developing the  
405 theoretical models, concrete is considered as a homogeneous material, thus abrupt variations in crack  
406 propagation rate are neglected. Irrespective of the variations observed in test data, a model based on  
407 the above-mentioned test data may still provide an averaged damage accumulation rate for the FC  
408 bonded joints under mode II dominated loading conditions, which can be considered as a conservative  
409 fatigue damage prediction model.

410 In addition, it is also clear that for FC bonded joints failing in cohesive failure within concrete, the  
411 mechanical properties of the concrete play a key role in damage initiation and propagation. The  
412 empirical constants in Eqs. (32) and (33) are obtained only from test data covering concrete strengths  
413 50MPa and 64.1MPa. Only two concrete strengths are far from sufficient to derive generally accurate  
414 empirical equations. Therefore, much more data covering different concrete strengths are required to  
415 develop more accurate functions for Eqs. (32) and (33). Nonetheless, the modelling approach  
416 presented in this paper is still generally applicable for all FC bonded joints.



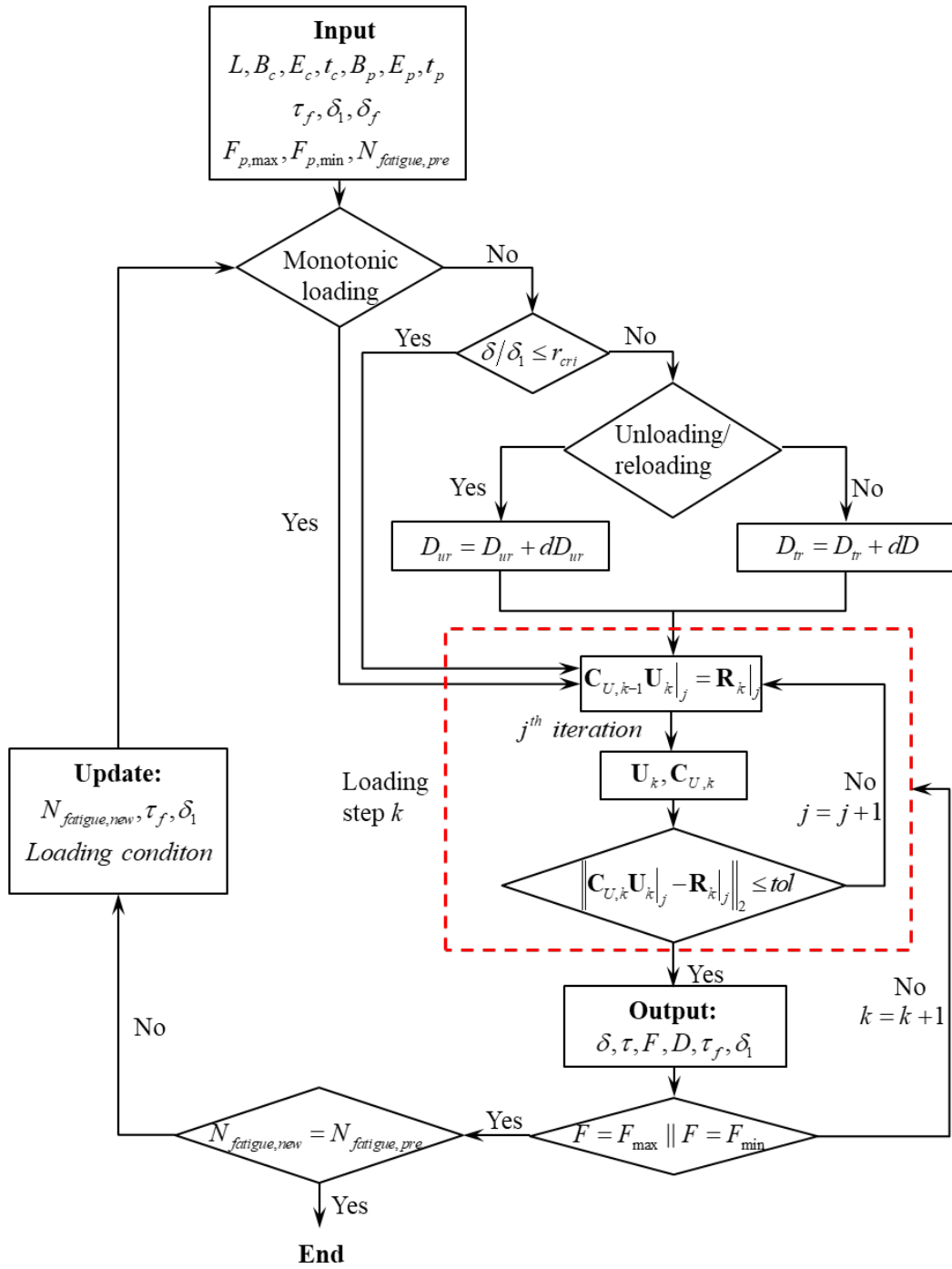
417

418 **Fig. 5.** The calibrated model for the damage accumulation rate of CFRP-to-concrete (FC) bonded  
 419 joints.

420 **5 Numerical implementation of the proposed model**

421 To demonstrate the numerical implementation of the proposed mode, the behaviour of a FC single-  
 422 shear pull-off test specimen under fatigue loading was modelled using the FD method presented in  
 423 Section 2. Damage evolution due to fatigue loading was calculated using the damage accumulation  
 424 rate for unloading/reloading and transition stiffness given in Eqs (32) and (33). During the simulation,  
 425 the state of each node was checked at every loading cycle to determine if the node has reached the  
 426 range that fatigue damage starts to accumulate (i.e., node slip is greater than the critical ratio  $r_{cri}$ ).  
 427 Damage accumulation was initiated when reloading occurred. A flow diagram illustrating the  
 428 calculation algorithm implemented in Matlab [41] to simulate the behaviour of FC bonded joints  
 429 under mode II fatigue loading is given in Fig. 6.





430

431

**Fig. 6.** Flow chart of the numerical implementation of the proposed model.

432

In the algorithm shown in Fig. 6, the material properties ( $E_c$ ,  $E_p$ ), geometry of the bonded joints ( $B_p$ -

433

width of the FRP plate,  $L$ - length of the bonded joint,  $t_c$ -thickness of the concrete block,  $t_p$ -thickness

434

of the FRP plate), the initial parameters for the bond-slip relation ( $\tau_f$ - interfacial shear strength,  $\delta_1$ -

435

slip at interfacial shear strength,  $\delta_f$ -slip at full damage) under monotonic loading and the fatigue load

436

conditions ( $F_{max}$ -maximum applied load,  $F_{min}$ -minimum applied load,  $N_{fatigue,pre}$ -number of

437 predefined fatigue loading cycles) are given as input to start the analysis. When the bonded joint is  
 438 subjected to a monotonic loading condition, the  $\delta$  and  $\tau$  are calculated through an iterative process  
 439 for each force increment. The detailed solving process can be found in Ref. [34]. When the fatigue  
 440 loading is applied to the bonded joints and the maximum interfacial shear stress/slip has reached the  
 441 threshold value for fatigue damage accumulation (i.e.,  $\frac{\delta}{\delta_1} \geq r_{crt}$ ), the  $D_{ur}$ , and  $D_{tr}$  will be calculated  
 442 and updated for the subsequent calculation. These damage parameters will be further used as input  
 443 for the iterative solution process. Once a converged solution is obtained (that is when  
 444  $\|\mathbf{C}_{U,k}\mathbf{U}_k|_j - \mathbf{R}_k|_j\|_2 \leq tol$ , where  $tol$  is the tolerance value to accept the convergence), the  
 445 interfacial slip, stress, damage parameters, and the parameters for the bond-slip relation in the current  
 446 loading cycle will be used for the subsequent calculation. In each loading cycle, such process will be  
 447 repeated until the prescribed force is attained. The above process will be looped until the number of  
 448 loading cycles has reached the predetermined value.

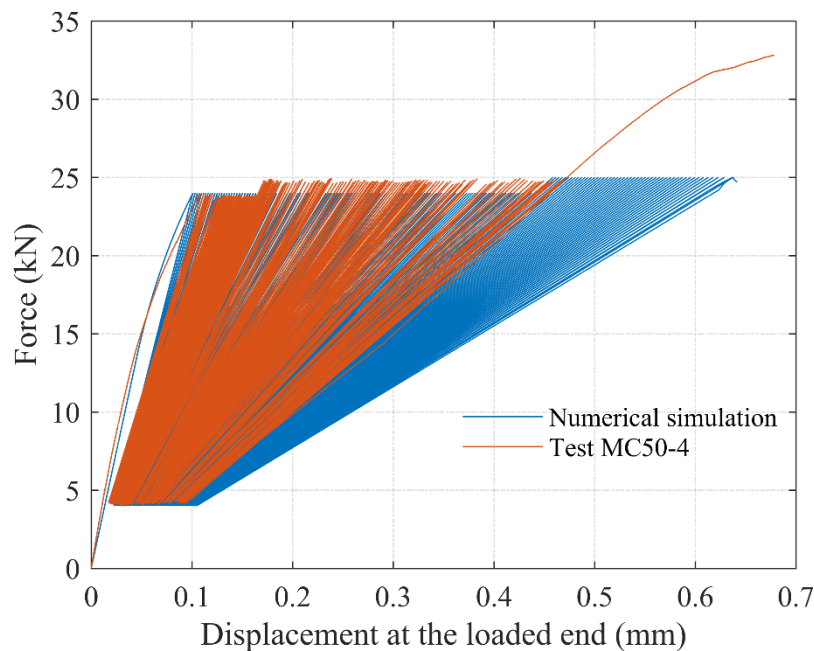
449 To demonstrate the workability of the proposed model and FD algorithm, behaviour of the specimen  
 450 MC50-4 from Zhou et al. [27] was simulated using the parameters given in Table. 1. In the numerical  
 451 simulation, the loading protocol followed in the test was used as the input to control the simulation.  
 452 The bonded joint was first monotonically loaded to 24kN and then unloaded to 4kN. This was then  
 453 followed by 2500 cycles of fatigue loading ranging from 4kN to 24kN. Next another 3000 cycles of  
 454 fatigue loading ranging from 4kN to 25kN were applied. Finally, monotonic loading was applied until  
 455 full debonding of the bonded joint occurred.

456 **Table 1.** Parameters used in the simulation of sample MC504

$E_p$	$b_p$	$t_p$	$E_c$	$b_c$	$t_c$	$\tau_{f,0}$	$\delta_1$	$\delta_2$	$L$
MPa	mm	mm	MPa	mm	mm	MPa	mm	mm	mm
160000	50	1.4	33446	150	200	7.24	0.045	0.27	300

457

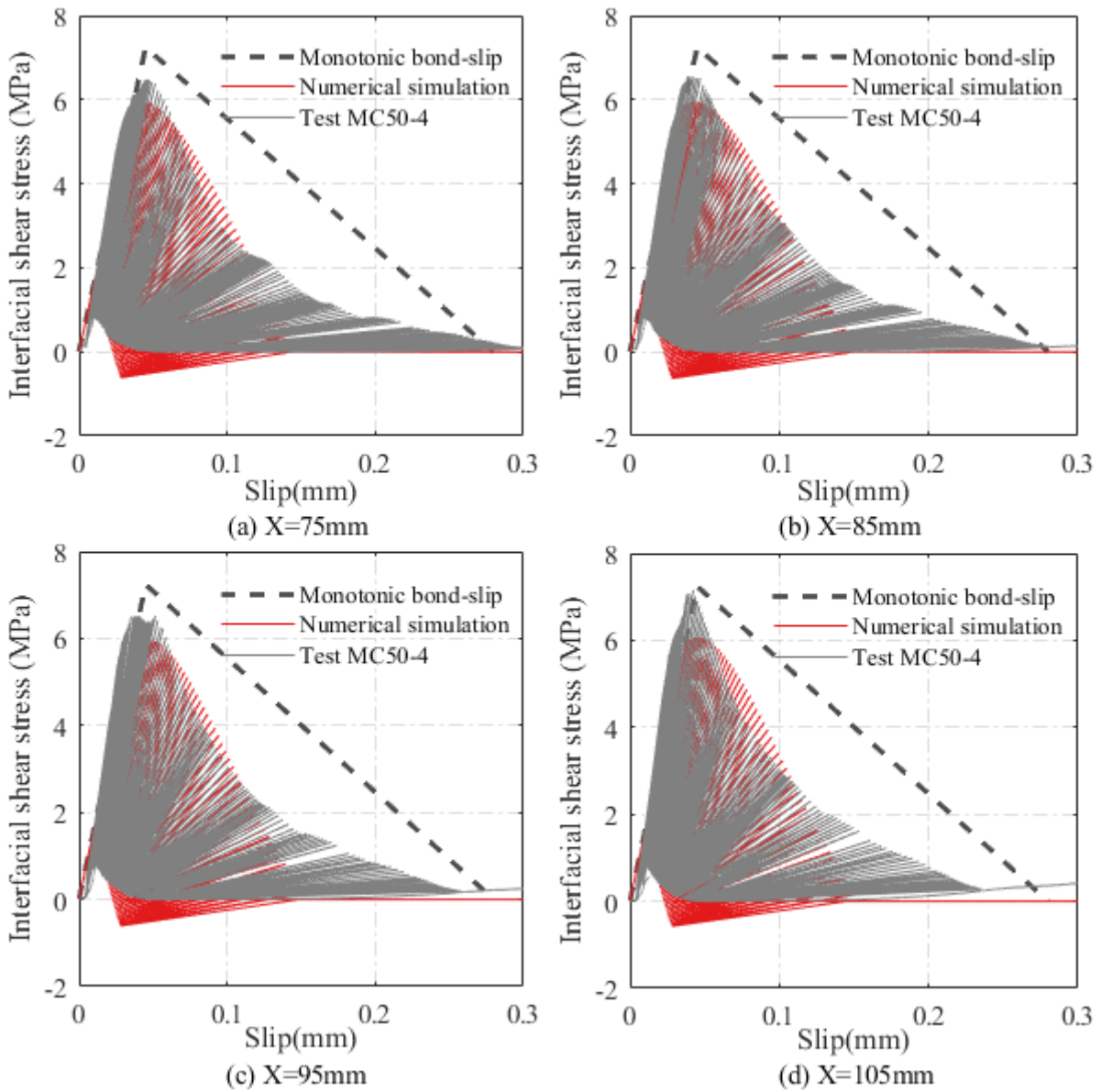
458 Fig. 7 presents the comparison between the experimental and numerical simulation results in terms  
459 of the load-displacement curve at the loaded end. It should be noted that the curves are plotted every  
460 20 cycles as the data was recorded at such frequency in the test. It is obvious that the displacement at  
461 the loaded end increased with the loading cycles while the slope of the curve decreased. However,  
462 compared to the experimental results, the damage accumulated much faster in the numerical  
463 simulation. Unlike the experimental test which failure occurred during the final monotonic loading,  
464 the numerical simulation shows that the bonded joint failed when the number of loading cycles was  
465 3500. Such a difference was expected as the proposed model used a faster damage accumulation rate  
466 than what was observed in the experiments within the bond length closer to the loaded end. Therefore,  
467 predictions tend to provide conservative results. To account for the effects of the compressive/tensile  
468 stresses within the bonded joints on the fatigue bond behaviour, the damage accumulation rate must  
469 consider the mode mix ratio. Such a model can only be developed once experimental data under  
470 mixed mode loading becomes available. However, this is outside the scope of the present study.



472 **Fig. 7.** Comparison between numerical simulation and test.

473 Since the proposed model is aimed at modelling the bond behaviour under mode II loading, only the  
474 bond bond-slip curves and damage parameter evolution at 75mm, 85mm, 95mm and 105mm away

475 from the loaded end from both experimental test and numerical simulation are compared in Figs. 8  
476 and 9. In the simulation, it is obvious that negative shear stresses occurred in the fatigue loading  
477 cycles. Such behaviour is consistent with the experimental findings presented in Zhou et al. [14] for  
478 FC bonded joints subjected to cyclic loading. However, interfacial shear stress is always positive in  
479 the experimental test results of the fatigue test specimens, as a direct result of the regression analysis  
480 method used in obtaining the strain distribution [26]. In obtaining the data from experimental results,  
481 noise of data was filtered using a monotonic mathematical expression-based regression analysis  
482 method. In doing so, some of the local peaks and valleys (especially if the values are relatively small)  
483 in the strain distribution along the bond length were smoothed. Such smoothing is believed to be  
484 the reason for not obtaining negative shear stress values, which were clearly present in experimental  
485 results of cyclic loading of similar bonded joints [14]. Nonetheless, error caused by the regression  
486 analysis is significant only at the later stages of the bond-slip curve when the shear stress reaches zero  
487 and the damage parameter is close to 1. Therefore, the overall effect of this error on the global  
488 behaviour was considered to be negligible.

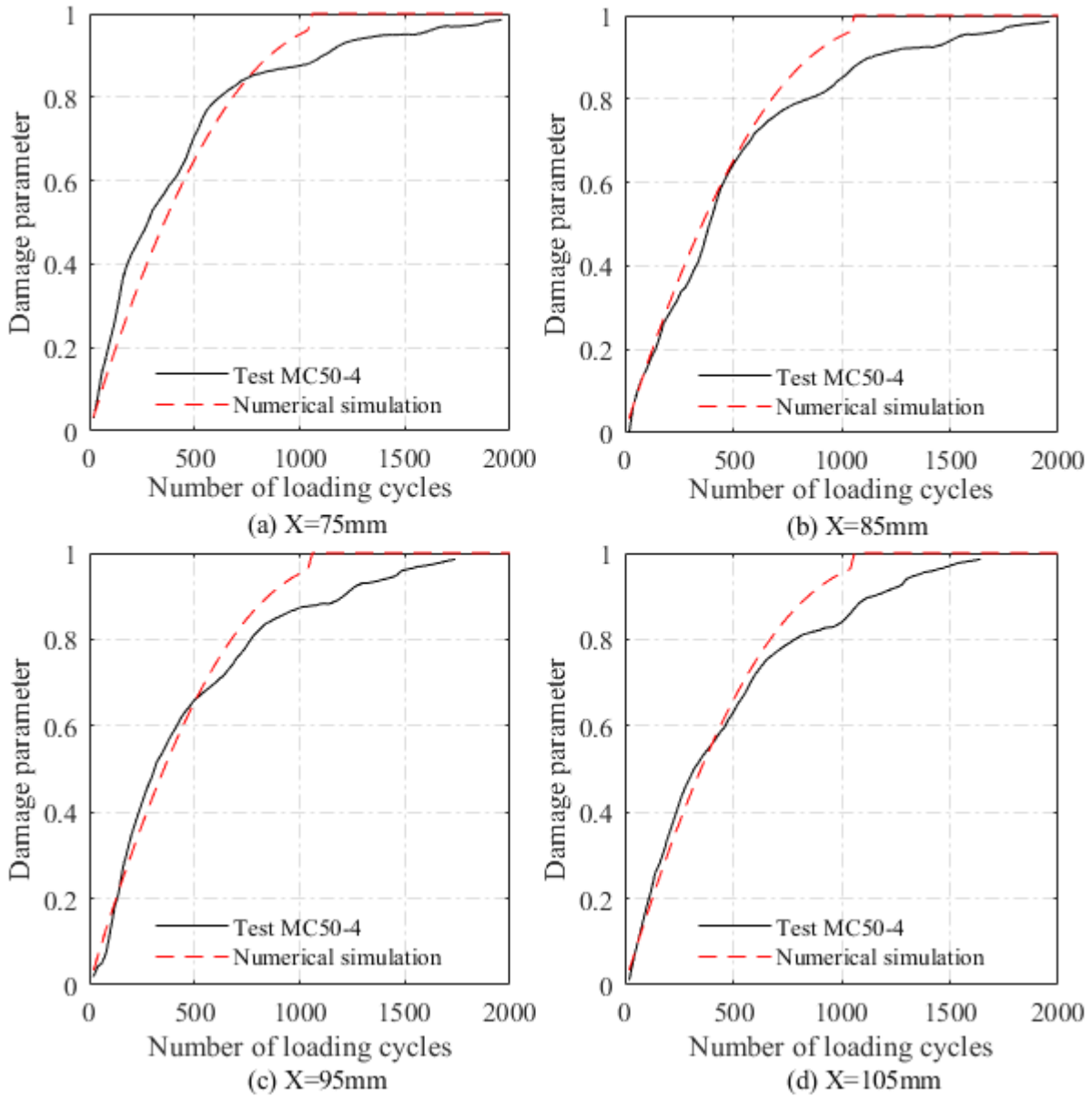


489

490 **Fig.8.** Comparison of the bond-slip relation between numerical simulation and test MC30-4 at  
 491 different locations.

492 Experimental results of the damage parameter evolution showed a good agreement with the  
 493 simulation results while the damage parameter is less than 0.8 (Fig. 9). It is assumed that full damage  
 494 at a node is reached when either the maximum interfacial shear stress value become negative or when  
 495 a node enters the reversed softening region (Fig. 9). This assumption is employed to ensure the  
 496 ultimate stress is not negative when the damage parameter reaches 1 during the simulation. As a result  
 497 of this assumption, a jump in the damage parameter was observed from approximately 0.9 to 1 in the  
 498 simulation results. For all the experimental data used to calibrate the models proposed in this paper,

499 the maximum loading amplitude was over 65% of the bond strength. Therefore, strict application of  
500 the model is also limited to the loading range of the tests, i.e., over 65% of the bond strength. When  
501 the maximum load amplitude is over 65% of the bond strength, the damage parameter can expected  
502 to be closer to 1 when the maximum shear stress becomes zero. As such, assuming full damage is  
503 deemed to be reasonable.



504  
505 **Fig. 9.** Comparison of the unloading/reloading damage parameter evolution between numerical  
506 simulation and test MC30-4 at different locations.

## 507 **6 Conclusions**

508 In this paper, a numerical model which can predict the bond behaviour of CFRP-to-concrete (FC)  
509 bonded joints failing in cohesion failure within concrete under mode II fatigue loading was developed.  
510 Based on the comparison between numerical simulations and test results, the following conclusions  
511 can be drawn:

- 512 1. The fatigue damage accumulation rate was found to vary along the bond length. Fatigue  
513 damage accumulation rate closer to the loaded end was much slower than that in regions far  
514 away from the loaded end. This low fatigue damage accumulation rate closer to the loaded  
515 end is attributed to the existence of compressive stresses in the regions close to the loaded end.
- 516 2. It was found that even though the damage level and the applied stress amplitude are the same,  
517 the damage accumulation rate at different locations could be different. This is due to brittle,  
518 unstable cracking within concrete which are typically not distributed uniformly along the bond  
519 length.
- 520 3. The damage accumulation rate for the unloading/reloading and transition stiffness were  
521 calibrated as a relation between the damage level and the stress amplitude by using the bond-  
522 slip relation in regions with mode II dominant loading. Such a model can be used to predict  
523 the bond-behaviour of FC bonded joints under mode II fatigue loading.
- 524 4. The proposed numerical simulation slightly overestimates the debonding rate and thus  
525 provides a conservative prediction for the fatigue life of the bonded joints. This is due to  
526 ignoring the beneficial effects from the compressive stresses near the loaded end on reducing  
527 the rate of crack propagation, which was done as only mode II loading was considered in the  
528 present study. For pure mode II load conditions, the proposed numerical simulation is  
529 expected to provide more accurate predictions.
- 530 5. A larger test database on the bond behaviour of FC bonded joints under fatigue loading is  
531 required to further calibrate and improve the accuracy of the proposed model. In addition,

532 while the present study is focused on cohesion failure within concrete, numerical models for  
533 other interfacial failure modes are worth investigation in future studies.

#### 534 **Acknowledgement**

535 The authors are thankful for the financial support received from the Natural Science Foundation of  
536 Hunan Province, China (Grant No. 2021JJ40777) to the first author.

#### 537 **Reference**

- 538 [1]. Hollaway, LC and Teng JG. Strengthening and rehabilitation of civil Infrastructures using  
539 fibre-reinforced polymer (FRP) composites. 2008: Elsevier Science.
- 540 [2]. de Waal, L, Fernando D, Nguyen VT, Cork R, and Foote J. FRP strengthening of 60 year old  
541 pre-stressed concrete bridge deck units. *Eng. Struct.*, 2017. 143: p. 346-357.
- 542 [3]. Chen, GM, Chen JF, and Teng JG. Behaviour of FRP-to-concrete interfaces between two  
543 adjacent cracks: A numerical investigation on the effect of bondline damage. *Constr. Build.*  
544 *Mater.*, 2012. 28(1): p. 584-591.
- 545 [4]. Chen, JF and Teng JG. Anchorage strength models for FRP and steel plates attached to  
546 concrete. *J. Struct. Eng.*, 2001. 127(7): p. 784-791.
- 547 [5]. Lu, XZ, Teng JG, Ye LP, and Jiang JJ. Bond–slip models for FRP sheets/plates bonded to  
548 concrete. *Eng. Struct.*, 2005. 27(6): p. 920-937.
- 549 [6]. Tao, Y and Chen JF. Concrete damage plasticity model for modeling FRP-to-concrete bond  
550 behavior. *J. Compos. Constr.*, 2014. 19(1).
- 551 [7]. Yuan, H, Teng JG, Seracino R, Wu ZS, and Yao J. Full-range behavior of FRP-to-concrete  
552 bonded joints. *Eng. Struct.*, 2004. 26(5): p. 553-565.
- 553 [8]. Yao, J, Teng JG, and Chen JF. Experimental study on FRP-to-concrete bonded joints. *Compos.*  
554 *B. Eng.*, 2005. 36(2): p. 99-113.
- 555 [9]. Martinelli, E and Caggiano A. Low-Cycle Fatigue of FRP Strips Glued to a Quasi-Brittle  
556 Material. *Materials (Basel, Switzerland)*, 2021. 14(24).
- 557 [10]. Mazzotti, C, Savoia M, and Ferracuti B. A new single-shear set-up for stable debonding of  
558 FRP–concrete joints. *Constr. Build. Mater.*, 2009. 23(4): p. 1529-1537.
- 559 [11]. Ko, H and Sato Y. Bond stress-slip relationship between FRP sheets and concrete under cyclic  
560 load. *J. Compos. Constr.*, 2007. 11(4): p. 419-426.
- 561 [12]. Martinelli, E and Caggiano A. A unified theoretical model for the monotonic and cyclic  
562 response of FRP strips glued to concrete. *Polymers*, 2014. 6(2): p. 370-381.



- 563 [13]. Carrara, P and De Lorenzis L. A coupled damage-plasticity model for the cyclic behavior of  
564 shear-loaded interfaces. *J. Mech. Phys. Solids*, 2015. 85(1): p. 33-53.
- 565 [14]. Zhou, H, Fernando D, Chen GM, and Kitipornchai S. The quasi-static cyclic behaviour of  
566 CFRP-to-concrete bonded joints: An experimental study and a damage plasticity model. *Eng.*  
567 *Struct.*, 2017. 153: p. 43-56.
- 568 [15]. Mazzotti, C and Savoia M. FRP-concrete bond behaviour under cyclic debonding force. *Adv.*  
569 *Struct. Eng*, 2009. 12(6): p. 771-780.
- 570 [16]. Gao, WY, Teng JG, and Dai JG. Effect of temperature variation on the full-range behavior of  
571 FRP-to-concrete bonded joints. *J. Compos. Constr.*, 2012. 16(6): p. 671-683.
- 572 [17]. Bizindavyi, L, Neale KW, and Erki MA. Experimental investigation of bonded fiber  
573 reinforced polymer-concrete joints under cyclic loading. *J. Compos. Constr.*, 2003. 7(2): p.  
574 127-134.
- 575 [18]. Diab, HM, Wu ZS, and Iwashita K. Theoretical solution for fatigue debonding growth and  
576 fatigue life prediction of FRP-concrete interfaces. *Adv. Struct. Eng*, 2009. 12(6): p. 781-792.
- 577 [19]. Carloni, C, Subramaniam KV, Savoia M, and Mazzotti C. Experimental determination of  
578 FRP-concrete cohesive interface properties under fatigue loading. *Compos. Struct.*, 2012.  
579 94(4): p. 1288-1296.
- 580 [20]. Zhang, W. Experimental study on fatigue behaviour of CFRP plates externally bonded to  
581 concrete substrate. *Struct. Concr.*, 2016. 17(2): p. 235-244.
- 582 [21]. Zhang, W. Prediction of the bond-slip law between externally bonded concrete substrates and  
583 CFRP plates under fatigue loading. *Int. J. Civ. Eng.*, 2017.
- 584 [22]. Li, K, Cao SY, and Wang XL. Experimental study on the fatigue endurance of the CFRP-  
585 concrete interface. *J. Compos. Constr.*, 2014. 19(4): p. 04014075.
- 586 [23]. Li, K, Cao S, Yang Y, and Zhu J. Bond-slip relationship for CFRP sheets externally bonded  
587 to concrete under cyclic loading. *Materials (Basel, Switzerland)*, 2018. 11(3).
- 588 [24]. Yun, YC, Wu YF, and Tang WC. Performance of FRP bonding systems under fatigue loading.  
589 *Eng. Struct.*, 2008. 30(11): p. 3129-3140.
- 590 [25]. Ferrier, E, Bigaud D, Hamelin P, Bizindavyi L, and Neale K. Fatigue of CFRPs externally  
591 bonded to concrete. *Mater. Struct.*, 2005. 38(1): p. 39-46.
- 592 [26]. Zhu, JT, Wang XL, Kang XD, and Li K. Analysis of interfacial bonding characteristics of  
593 CFRP-concrete under fatigue loading. *Constr. Build. Mater.*, 2016. 126: p. 823-833.
- 594 [27]. Zhou, H, Fernando D, Thuan Nguyen V, and Dai J-G. The bond behaviour of CFRP-to-  
595 concrete bonded joints under fatigue cyclic loading: An experimental study. *Constr. Build.*  
596 *Mater.*, 2021. 273: p. 121674.

- 597 [28]. Carloni, C and Subramaniam KV. Investigation of sub-critical fatigue crack growth in  
598 FRP/concrete cohesive interface using digital image analysis. *Compos. B. Eng.*, 2013. 51: p.  
599 35-43.
- 600 [29]. Yuan, H, Luo G, Liu C, and Zeng L. Interfacial properties of CFRP sheets and concrete  
601 subjected to variable amplitude fatigue loading. *Struct. Concr.*, 2021.
- 602 [30]. Al-Saoudi, A, Al-Mahaidi R, Kalfat R, and Cervenka J. Finite element investigation of the  
603 fatigue performance of FRP laminates bonded to concrete. *Compos. Struct.*, 2019. 208: p.  
604 322-337.
- 605 [31]. Chalot, A, Michel L, and Ferrier E. Experimental study of external bonded CFRP-concrete  
606 interface under low cycle fatigue loading. *Compos. B. Eng.*, 2019. 177.
- 607 [32]. Wei, MW, Xie JH, Huang PY, and Huang KH. Fatigue behaviour of the bond interface  
608 between carbon fibre - reinforced polymer sheets and concrete. *Fatigue Fract. Eng. Mater.*  
609 *Struct.*, 2020. 43(9): p. 2116-2129.
- 610 [33]. Zhang, W, Tang Z, Yang Y, Wei J, and Stanislav P. Mixed-mode debonding behavior between  
611 CFRP plates and concrete under fatigue loading. *J. Struct. Eng.-ASCE*, 2021. 147(5): p.  
612 04021055.
- 613 [34]. Carrara, P and Ferretti D. A finite-difference model with mixed interface laws for shear tests  
614 of FRP plates bonded to concrete. *Compos. B. Eng.*, 2013. 54: p. 329-342.
- 615 [35]. Roe, KL and Siegmund T. An irreversible cohesive zone model for interface fatigue crack  
616 growth simulation. *Eng. Fract. Mech.*, 2003. 70(2): p. 209–232.
- 617 [36]. Lu, XZ, Ye LP, Teng JG, and Jiang JJ. Meso-scale finite element model for FRP sheets/plates  
618 bonded to concrete. *Eng. Struct.*, 2005. 27(4): p. 564-575.
- 619 [37]. Zhou, H. Behaviour of FRP-to-concrete bonded joints under cyclic and thermal loading, in  
620 School of Civil Engineering. 2019, The University of Queensland: Brisbane, Australia.
- 621 [38]. Lin, JP and Wu YF. Numerical analysis of interfacial bond behavior of externally bonded  
622 FRP-to-concrete joints. *J. Compos. Constr.*, 2016. 20(5): p. 04016028.
- 623 [39]. Fernando, D. Bond behaviour and debonding failures in CFRP-strengthened steel members,  
624 in Department of Civil and Structural Engineering. 2010, The Hong Kong Polytechnic  
625 University: HongKong, China.
- 626 [40]. Zhou, YW, Wu YF, and Yun YC. Analytical modeling of the bond–slip relationship at FRP-  
627 concrete interfaces for adhesively-bonded joints. *Compos. B. Eng.*, 2010. 41(6): p. 423-433.
- 628 [41]. The Mathworks Inc. MATLAB version 9.3.0.713579 (R2017b). 2017: Natick, Massachusetts.  
629